S1. Introduction

This supplemental contains additional data referenced in the main article. The stress-strain curves are presented from uniaxial tension tests at the following strain rates: 10%/s, 1%/s, 0.1%/s, and 0.01%/s, for the following LCE networks: polydomain, 30% parallel, 90% parallel, 30% perpendicular, and 90% perpendicular. The contour plots from 3D Digital Image Correlation (DIC) for representative tests and the quantification of variability for the data is presented. Section S2 provides engineering stress-strain curves from uniaxial tension tests for the repeated testing of the samples. Section S3 contains contour plots of $\frac{|E_{yy}-\bar{E}_{yy}|}{StdE_{yy}}$ calculated from 3D DIC for representative tests, at different points on the stress-strain curve during the soft stress response, where $\bar{E}_{yy}$ and $StdE_{yy}$ are the average and standard deviation of the axial Green Lagrange strain measured by 3D DIC. This section includes contour plots of the strain field calculated at the maximum applied stretch and normalized by the maximum applied Green-Lagrange strain, for the following LCE networks: polydomain, 30% parallel, 90% parallel, and 30% perpendicular. The 90% perpendicular contour plots were calculated at about the start of hardening because it could not be imaged for greater values of strain. Finally, Section S3 includes analysis of the variability in the strain field computed as $\frac{StdE_{yy}}{\bar{E}_{yy}}$.

S2. Rate-dependent uniaxial tension response

The specimens were subjected to displacement controlled load-unload tests at different engineering strain rates ranging from 0.01%/s to 10%/s. One specimen was prepared for polydomain, 90% parallel, 30% perpendicular and 90% perpendicular, and used for tests at all strain rates to reduce the effect of specimen to specimen variability. Two specimens were used for the 30% parallel tests because the sample broke during testing. We repeated the tests for strain rates ranging from 0.01%/s to 10%/s for the polydomain specimen 2-5 times. For the 10%/s strain rate, 4 to 5 repetitions were done for 30% parallel and 90% parallel. For the 1%/s strain rate, 3 repetitions were done for 30% parallel. For the 0.1%/s strain rate, 2 repetitions were done for 30% perpendicular. Figures S1- S5 show the uniaxial stress-strain response for all the performed tests at different strain rates (10%/s, 1%/s, 0.1%/s, and 0.01%/s), for the polydomain (Fig. S1), 30% parallel (Fig. S2), 90% parallel (Fig. S3), 30% perpendicular (Fig. S4), and 90% perpendicular (Fig. S5). Comparing 10%/s, 1%/s, and 0.1%/s, the variations in the curves between strain rates were greater than the variation between repetitions. Additionally, the stress-strain curves did systematically stiffen or soften with repeated testing.

S3. 3D-DIC strain measurements

To investigate the spatial variability in the strain field, color contours plots of $\frac{|E_{yy}-\bar{E}_{yy}|}{Std.E_{yy}}$ are shown in (Figs. S6-S8). The Green-Lagrange axial strain E_{yy} was measured by 3D-DIC at different points in the soft stress response. The $\bar{E}_{yy}$ is the spatial average Green-Lagrange axial strain calculated at different points during the soft stress response, and $StdE_{yy}$ is the corresponding standard deviation. The color contours are plotted over the undeformed configuration for the polydomain (Fig. S6), 30% perpendicular (Fig. S7) and 90% perpendicular (Fig. S8) specimens. The different points correspond to the following points on the loading stress-strain curves: 1- peak stress; 2- end of softening; 3- start of hardening; and 4- the maximum stretch. In the color contour, light blue and yellow indicate 2 and 3 standard deviations away from the mean in $\bar{E}_{yy}$. In the polydomain at 10%/s (Fig. S6(a)), regions of higher deviation from the mean appeared at the beginning of the soft stress response (point 1), reached a maximum at point 2, then gradually dispersed into smaller regions after point 3 corresponding to the end of the soft stress response (Fig. S6(a)). Plotting the deviation from the mean strain, rather than just the strain in Fig. 8, brings out more clearly the heterogenous strain patterns. The hererogeneous strain pattern did not appear at low strains for the 10%/s loading rate in Fig. 8 because the standard deviation was small. The evolution in the strain variability, where larger regions of lower deviation from the mean strain dispersed into smaller regions, was more evident at lower strain rates, where alternating bands of higher and lower are evident beginning at point 3, the start of hardening in the stress response. The 30% perpendicular specimen also exhibited a similar evolution in the strain patterns and variation with strain rate (S8. At the highest 10%/s strain rate, the strain pattern did not vary significantly with strain in the soft stress region. For smaller strains, initial larger light blue regions of lower deviation from the mean dispersed into smaller yellow bands of higher deviation
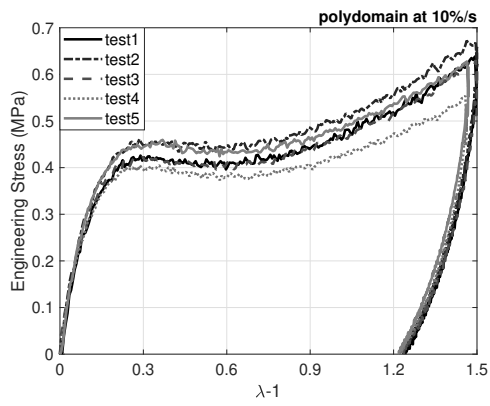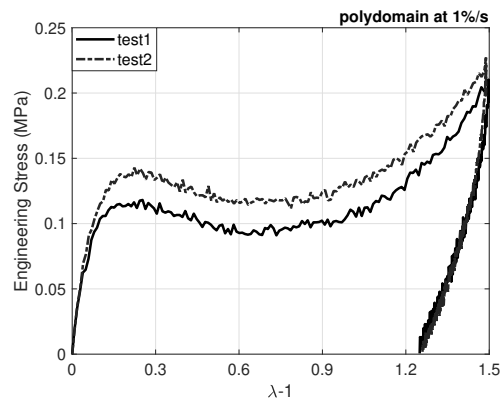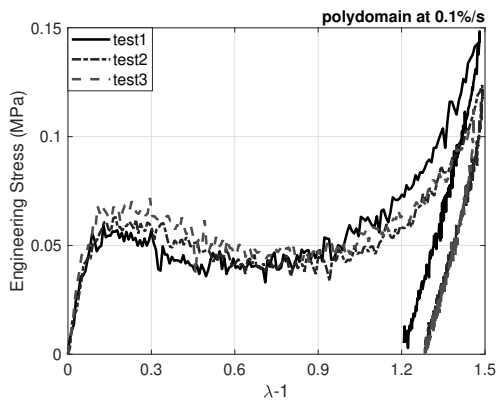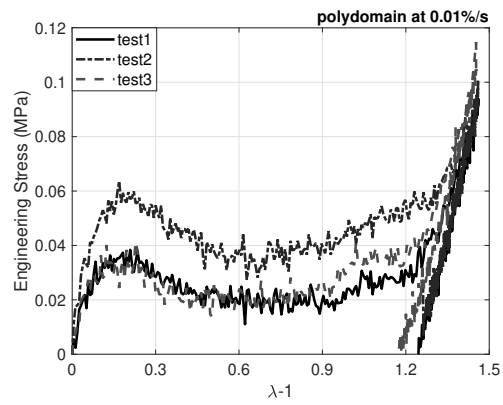
Figure S1: Uniaxial tension load-unload stress-strain response for polydomain and for all the tests numbered in the order that they were performed at strain rates: (a) 10%/s, (b) 1%/s, (c) 0.1%/s, and (d) 0.01%. The sample did not get stiffer over time and the variation was smaller than the variation between tests.
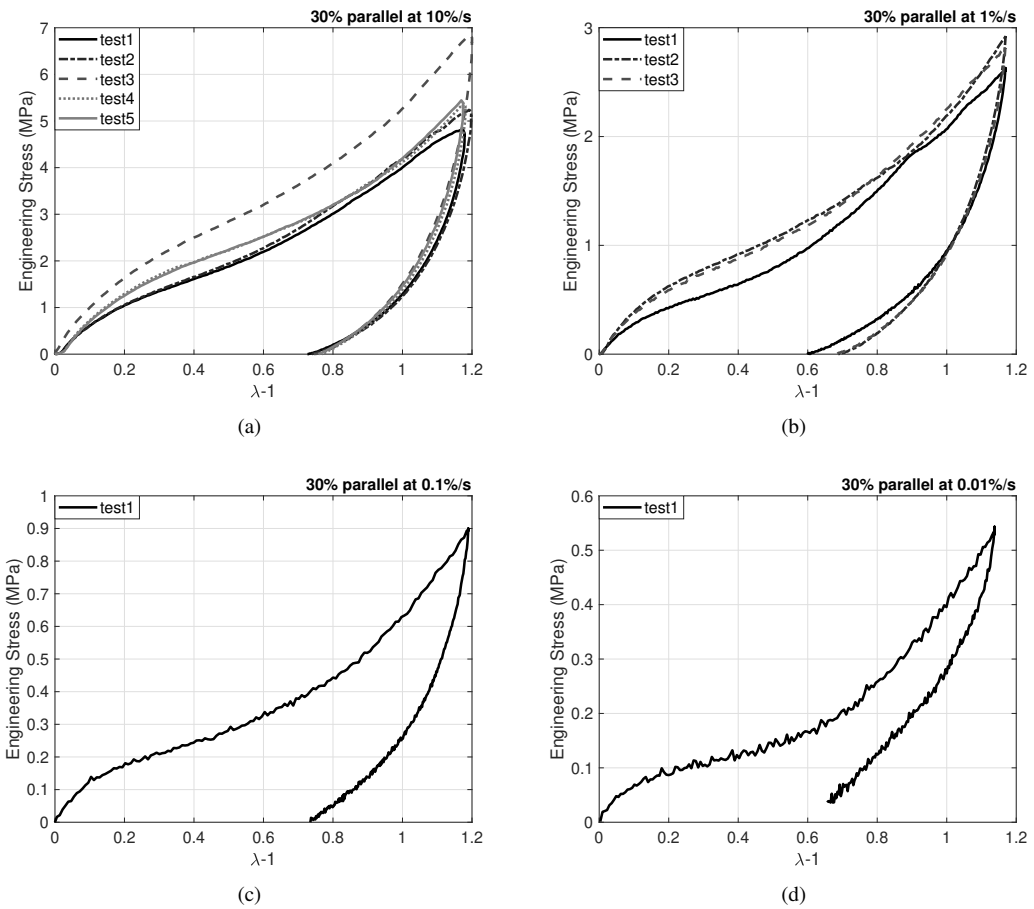
Figure S2: Uniaxial tension load-unload stress-strain response for 30% parallel and for all the tests numbered in the order that they were performed at strain rates: (a) 10%/s, (b) 1%/s, (c) 0.1%/s, and (d) 0.01%. The sample did not get stiffer over time and the variation was smaller than the variation between tests.
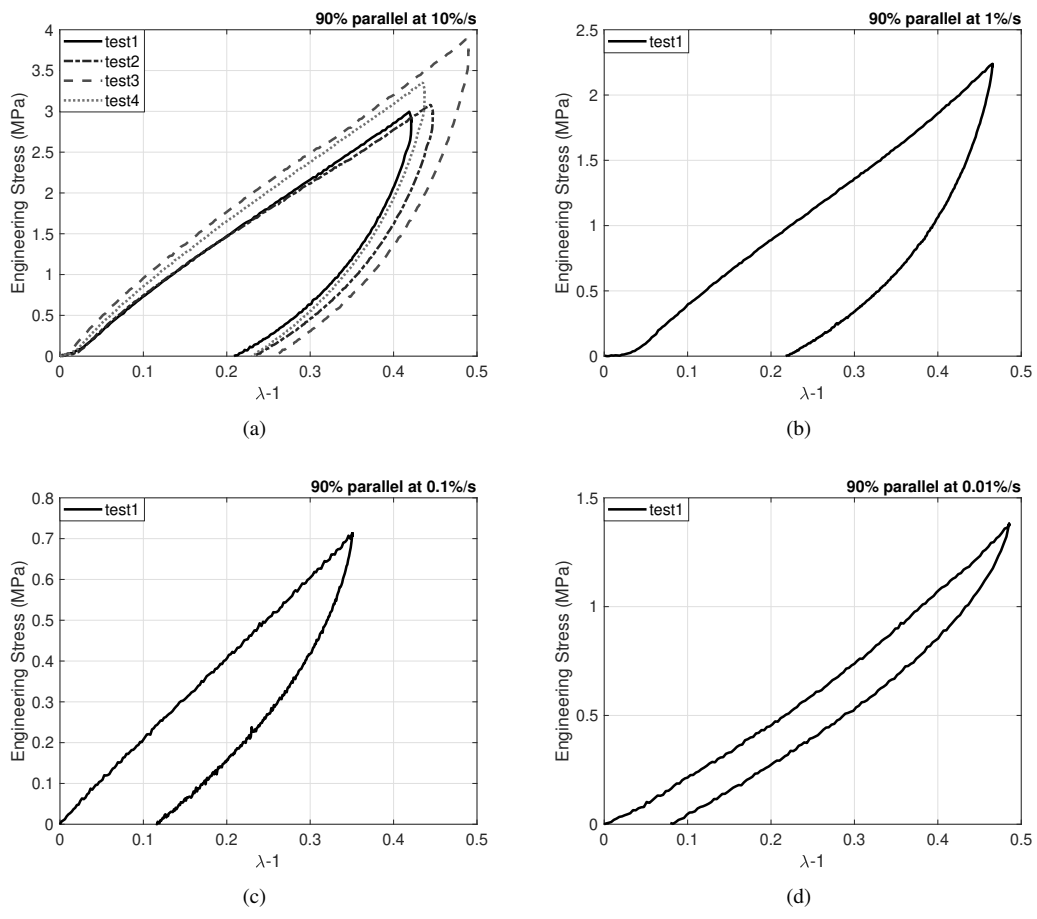
Figure S3: Uniaxial tension load-unload stress-strain response for 90% parallel and for all the tests numbered in the order that they were performed at strain rates: (a) 10%/s, (b) 1%/s, (c) 0.1%/s, and (d) 0.01%. The sample did not get stiffer over time and the variation was not larger than the variation between tests.
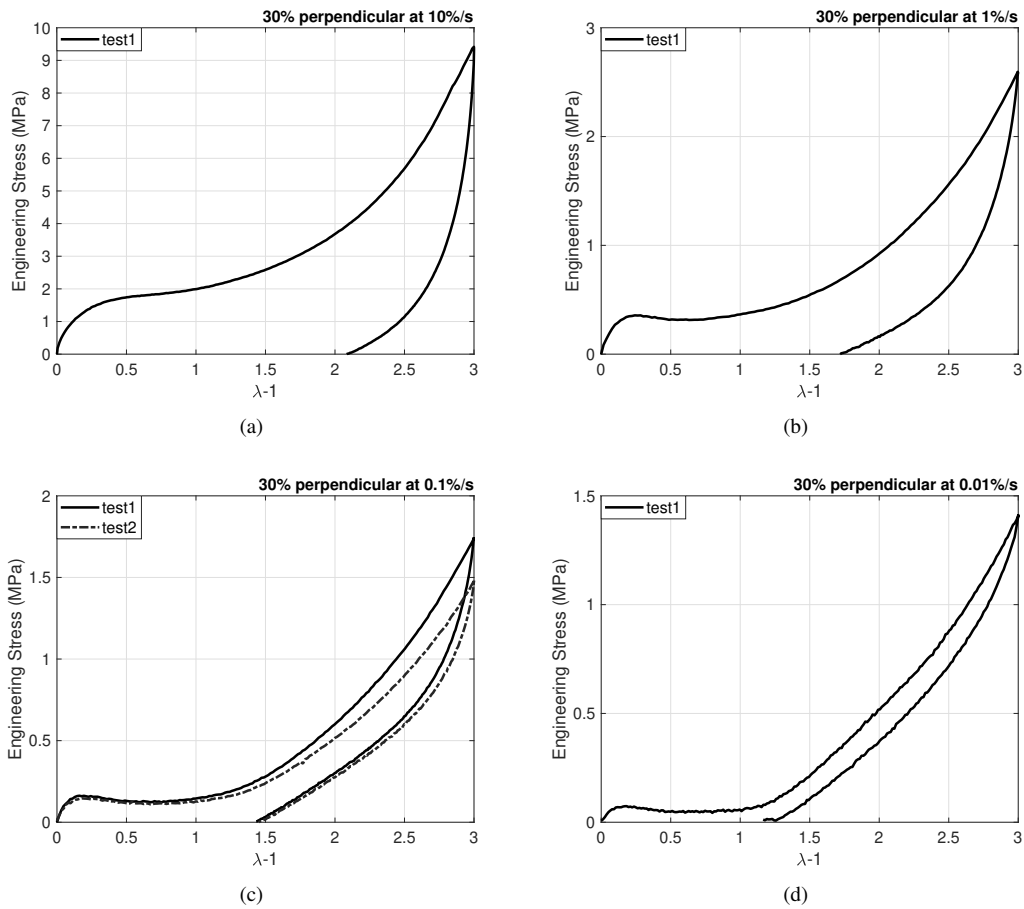
Figure S4: Uniaxial tension load-unload stress-strain response for 30% perpendicular and for all the tests numbered in the order that they were performed at strain rates: (a) 10%/s, (b) 1%/s, (c) 0.1%/s, and (d) 0.01%. The sample did not get stiffer over time and the variation was smaller than the variation between tests for the last tests at $0.1\%/s$
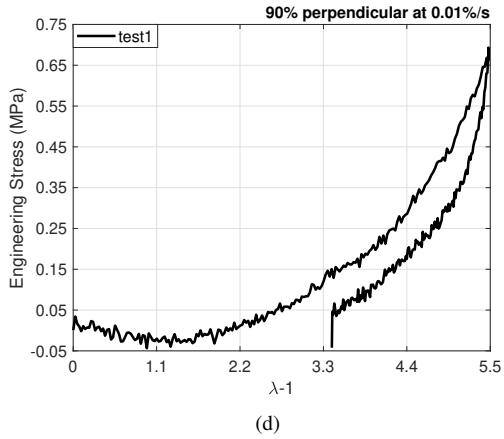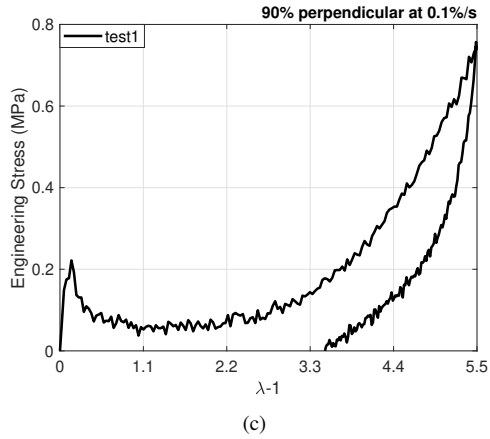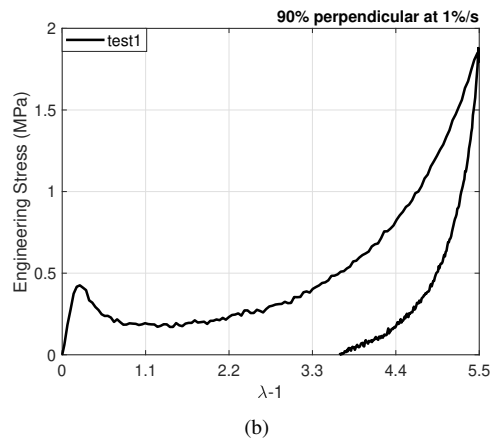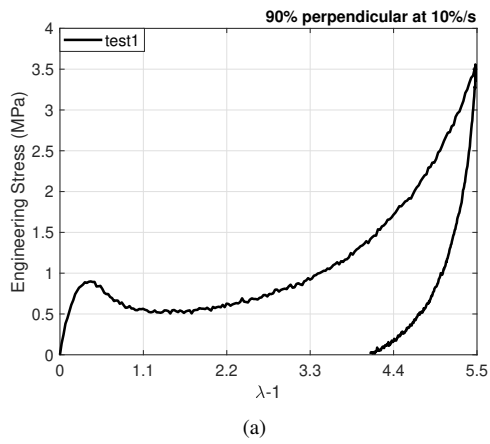
Figure S5: Uniaxial tension load-unload stress-strain response for 90% perpendicular and for all the tests numbered in the order that they were performed at strain rates: (a) 10%/s, (b) 1%/s, (c) 0.1%/s, and (d) 0.01%. Variability between tests was not tested in this sample.

from the mean at the end of the softening region. For the the 90% perpendicular specimen, regions with high deviation from the mean appeared at the boundaries of the specimen at the beginning of softening in point 1 then developed into more horizontal band-like structures.

The color contour plots of the Green-Lagrange axial (E_{yy}) and shear strains (E_{xy}) calculated by 3D-DIC at the maximum applied stretch, normalized by the maximum applied Green-Lagrange strain ε_{max}, are plotted for the different specimens at different strain rates in Fig. S9 - Fig. S12. For the 90% perpendicular specimen, the speckled region stretched outside of the field of view before the maximum applied stretch, and thus the plots for the 90% perpendicular specimen shows the strains calculated immediately before instance that the speckled region stretched outside of the camera field of view. In general, the strain fields were non-uniform for all network structures and loading directions. The polydomain showed a characteristic pattern of bands for the normalized uniaxial strain. For the 30% parallel specimen, the normalized axial strain and the normalized shear strain contours have diagonal bands for all the strain rates tested. This appeared in both specimens and all repeated tests for the 30% perpendicular material. The 90% parallel showed bands perpendicular to the direction of loading for the normalized axial strain and vertical bands for the normalized shear strain. The shear developed in 90% and 30% parallel specimens were significantly larger compared to polydomain and perpendicularly loaded samples.

The development of an inhomogeneous strain field was quantified by the standard deviation of the Green-Lagrange axial strain E_{yy} normalized by the spatial average of E_{yy} measured by 3D-DIC. Calculations are shown for the loading portion of all tests at 10%/s, 1%/s, 0.1%/s, and 0.01%/s strain rates for polydomain (Fig. S13), 30% parallel (Fig. S14), 90% parallel (Fig. S15), 30% perpendicular (Fig. S16), and 90% perpendicular (Fig. S17). The spatial variability of the strain contours were repeatably obtained in every test and the difference between each repeated test was smaller than the difference measured between different strain rates (Fig. S13 to Fig. S17).

10%/s

1%/s

(a)

(b)

0.1%/s

0.01%/s

$$\frac{|\mathbf{E_{yy}} - \bar{\mathbf{E}}_{\mathbf{yy}}|}{\mathbf{Std.E_{yy}}}$$

(c)

(d)
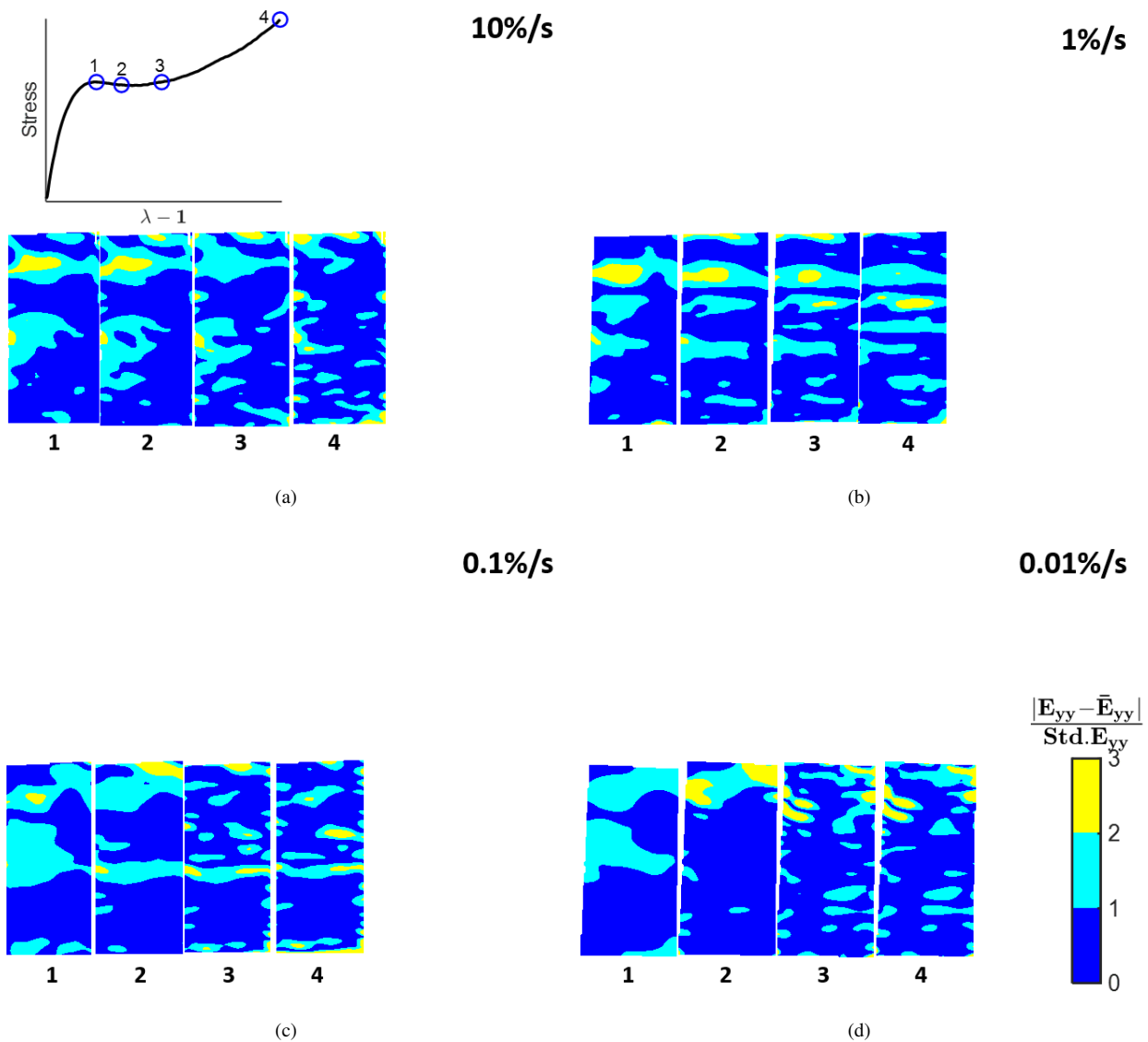
Figure S6: Strain contours for the variability in the strain contour measured as the number of standard deviations with respect to the mean, the specimen-averaged Green-Lagrange axial strain E_{yy} is measured using 3D DIC for representative tests of the polydomain samples at (a) 10%/s, (b) 1%/s, (c) 0.1%/s, and (d) 0.01% strain rates. An example of the stress-strain curve and the normalized variability with respect to E_{yy} curve is included to indicate four points in the soft stress response: 1- peak stress; 2- end of softening; 3-start of hardening; and 4- the maximum stretch. There is an increased variability in the strain field, becoming very localized during the soft stress response at $0.1\%/s$ and $0.01\%/s$ with deformation bands at $1\%/s$, however, hardly any pattern is formed at $10\%/s$.
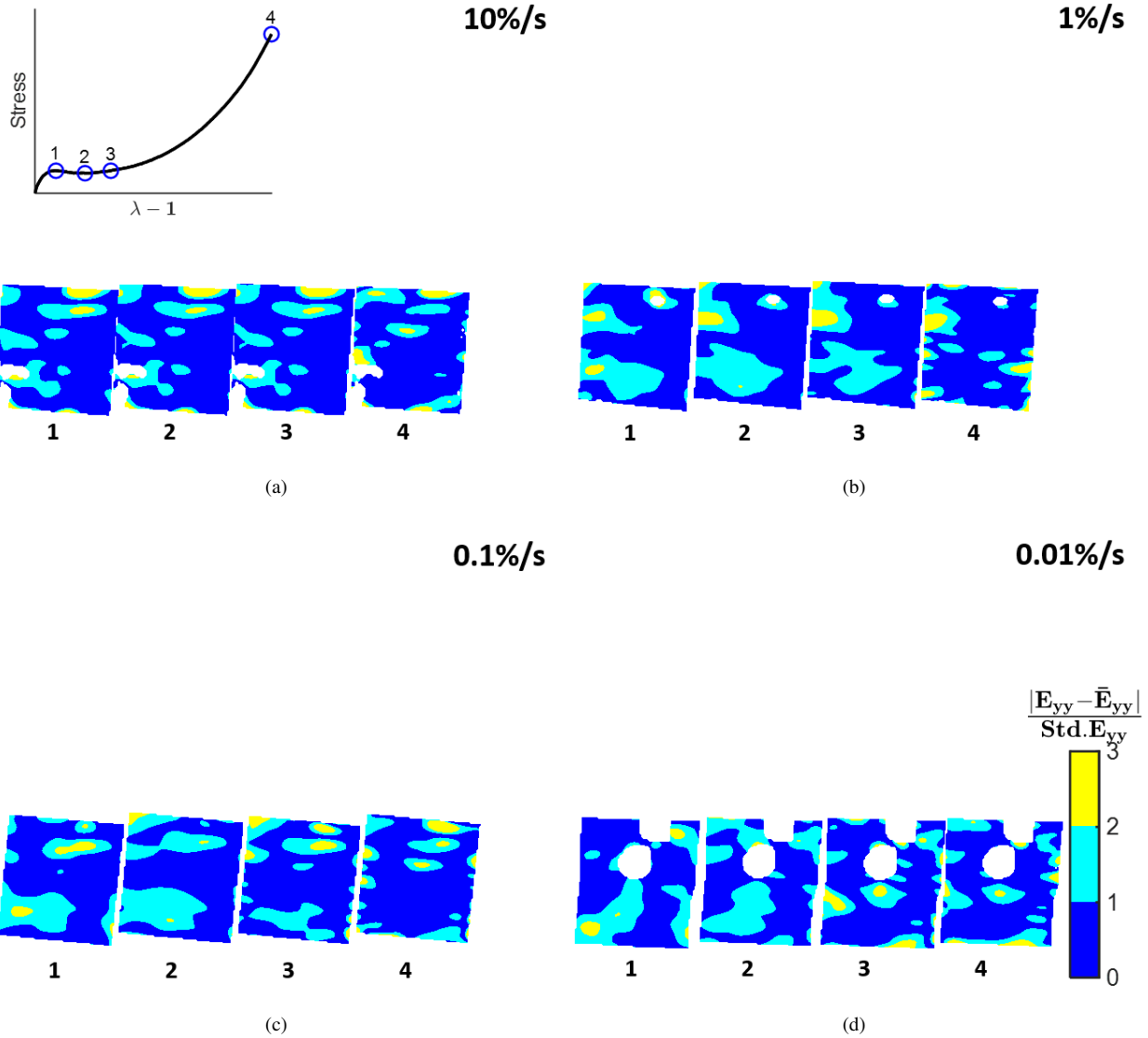
Figure S7: Strain contours for the variability in the strain contour measured as the number of standard deviations with respect to the mean, the specimen-averaged Green-Lagrange axial strain E_{yy} is measured using 3D DIC for representative tests of the 30% perpendicular samples at (a) 10%/s, (b) 1%/s, (c) 0.1%/s, and (d) 0.01% strain rates. An example of the stress-strain curve and the normalized variability with respect to E_{yy} curve is included to indicate four points in the soft stress response: 1- peak stress; 2- end of softening; 3-start of hardening; and 4- the maximum stretch. An evolving pattern was not observed at 10%/s because points 1-3 coincide, at $1\%/s$- $0.01\%/s$, the strain field evolves with an increased in variability from 1-2 that tends to decrease after 3.

9

10%/s

1%/s

0.1%/s

0.01%/s

$$\frac{|\mathbf{E}_{yy}-\bar{\mathbf{E}}_{yy}|}{\mathbf{Std}.\mathbf{E}_{yy}}$$

(a)

(b)

(c)

(d)
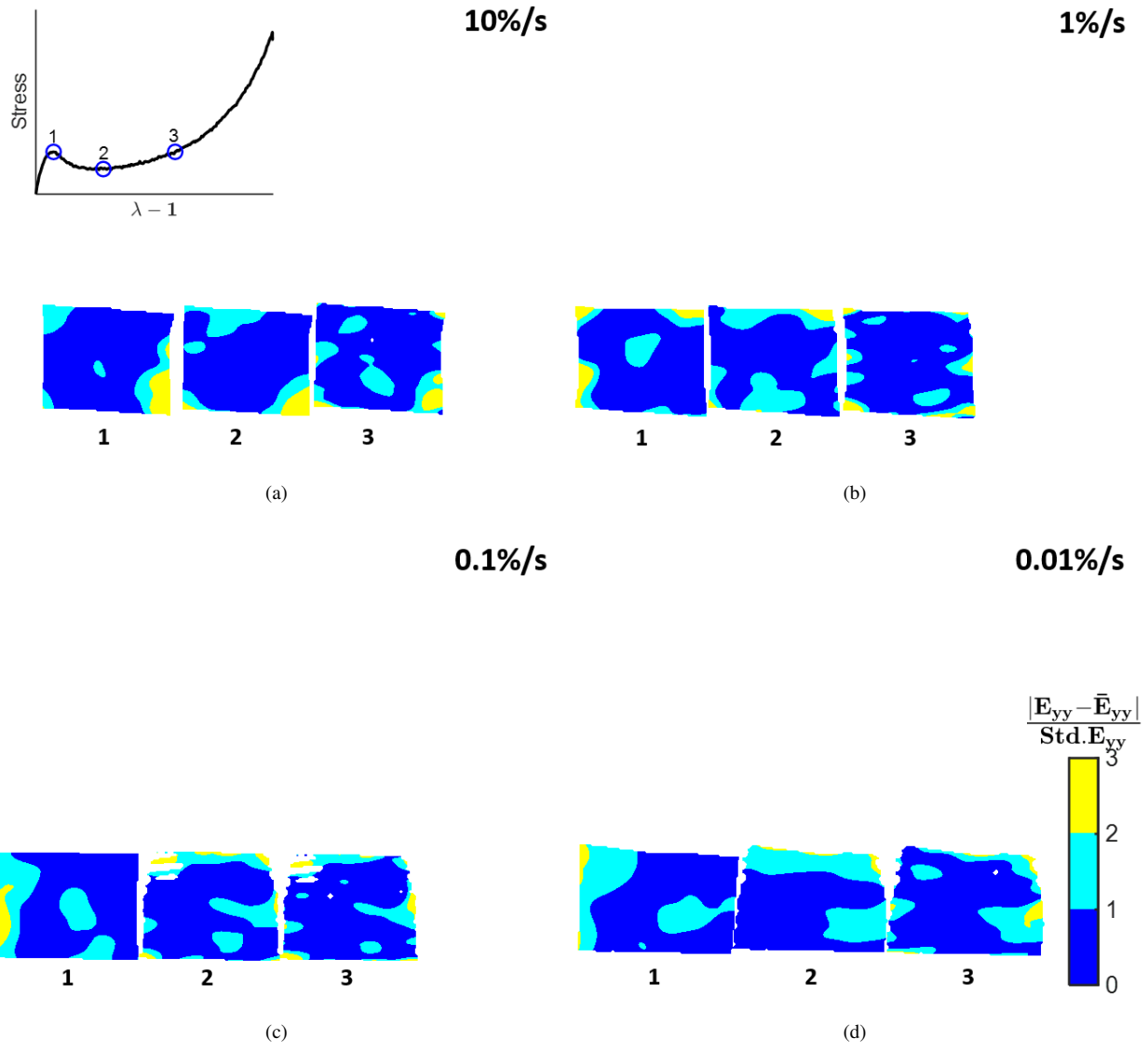
Figure S8: Strain contours for the variability in the strain contour measured as the number of standard deviations with respect to the mean, the specimen-averaged Green-Lagrange axial strain E_{yy} is measured using 3D DIC for representative tests of the 90% perpendicular samples at (a) 10%/s, (b) 1%/s, (c) 0.1%/s, and (d) 0.01% strain rates. An example of the stress-strain curve and the normalized variability with respect to E_{yy} curve is included to indicate four points in the soft stress response: 1- peak stress; 2- end of softening; 3-start of hardening; and 4- the maximum stretch. For all strain rates, the there is an increase in variability from 1 to 2, and starts decreasing at 3.
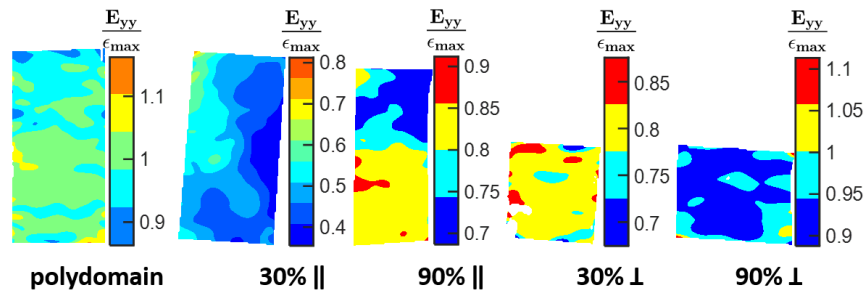
(a)
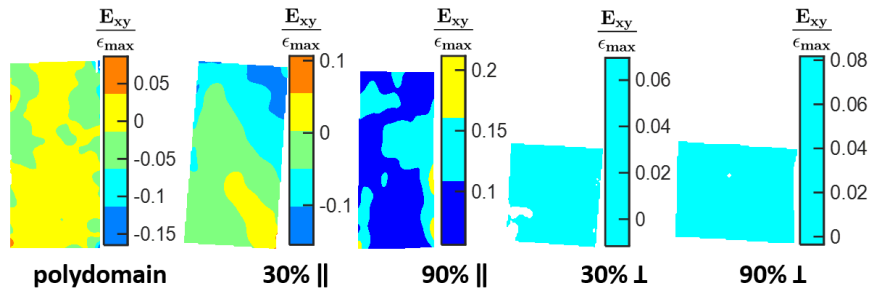
(b)

Figure S9: Strain contours for the Green-Lagrange axial strain E_{yy} normalized by the maximum applied strain (a) and for the Green-Lagrange shear strain E_{xy} normalized by the maximum applied strain. E_{yy} and E_{xy} were measured using 3D DIC for representative tests of all the LCE networks at the maximum applied stretch from tensile experiments at 10%/s. The contour plots show shear bands that may develop due to the alignment mesogen domains or network alignment, and that propagate in the principal direction, inducing variability in the axial strain field.
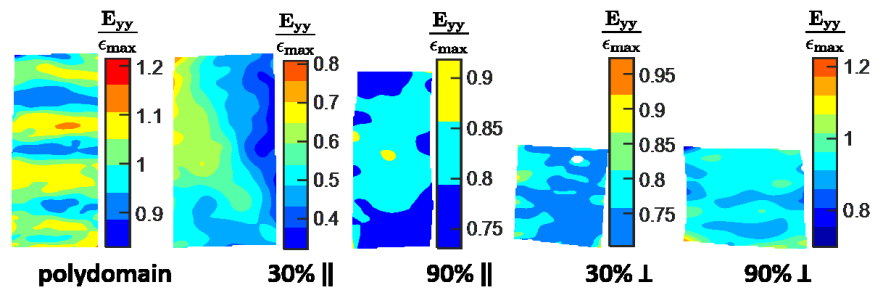
(a)
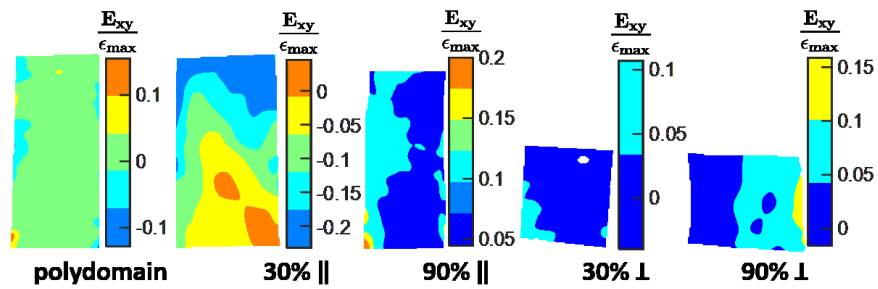
(b)

Figure S10: Strain contours for the Green-Lagrange axial strain E_{yy} normalized by the maximum applied strain (a) and for the Green-Lagrange shear strain E_{xy} normalized by the maximum applied strain, E_{yy} and E_{xy} were measured using 3D DIC for representative tests of all the LCE networks at the maximum applied stretch from tensile experiments at 1%/s. The contour plots show shear bands that may develop due to the alignment mesogen domains or network alignment, and that propagate in the principal direction, inducing variability in the axial strain field.
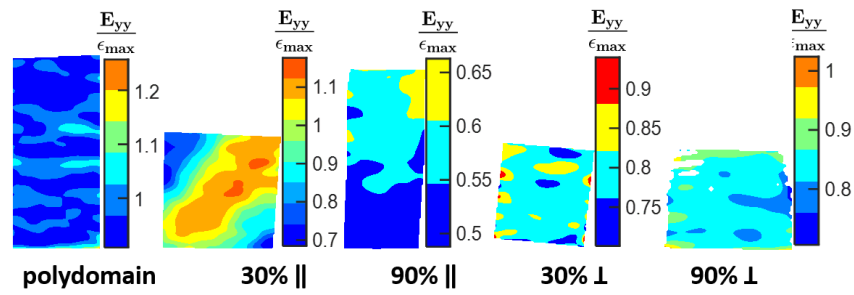
(a)
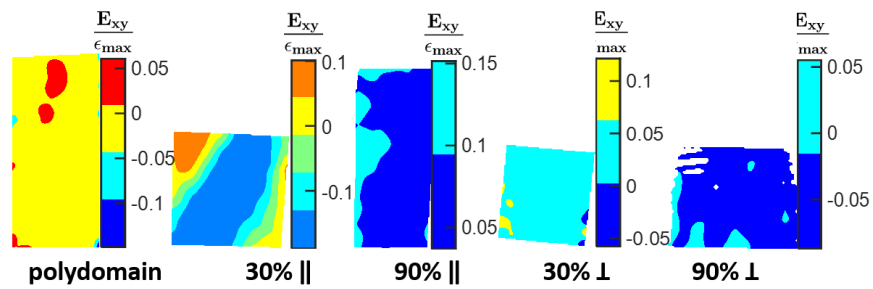
(b)

Figure S11: Strain contours for the Green-Lagrange axial strain E_{yy} normalized by the maximum applied strain (a) and for the Green-Lagrange shear strain E_{xy} normalized by the maximum applied strain, E_{yy} and E_{xy} were measured using 3D DIC for representative tests of all the LCE networks at the maximum applied stretch from tensile experiments at 0.1%/s. The contour plots show shear bands that may develop due to the alignment mesogen domains or network alignment, and that propagate in the principal direction, inducing variability in the axial strain field.
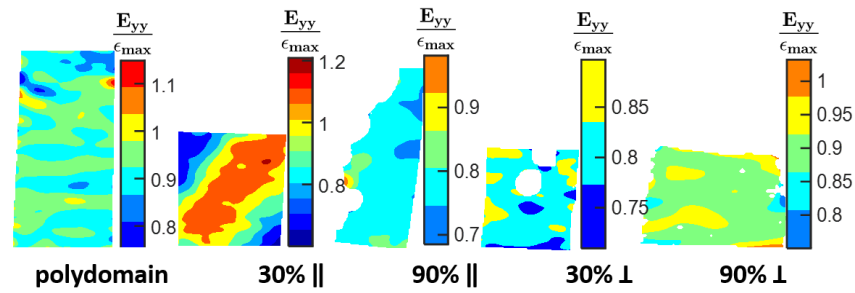
(a)
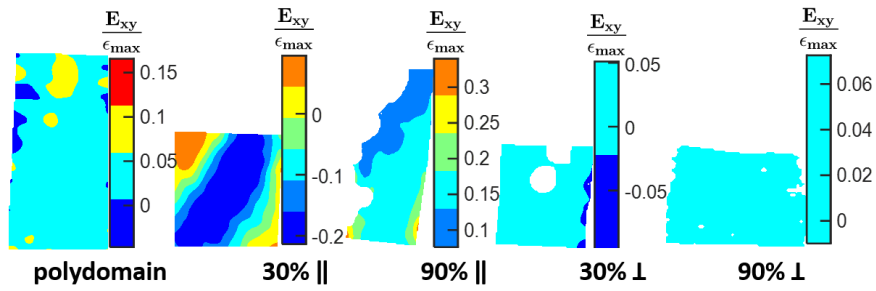
(b)

Figure S12: Strain contours for the Green-Lagrange axial strain E_{yy} normalized by the maximum applied strain (a) and for the Green-Lagrange shear strain E_{xy} normalized by the maximum applied strain, E_{yy} and E_{xy} were measured using 3D DIC for representative tests of all the LCE networks at the maximum applied stretch from tensile experiments at 0.01%/s. The contour plots show shear bands that may develop due to the alignment mesogen domains or network alignment, and that propagate in the principal direction, inducing variability in the axial strain field.
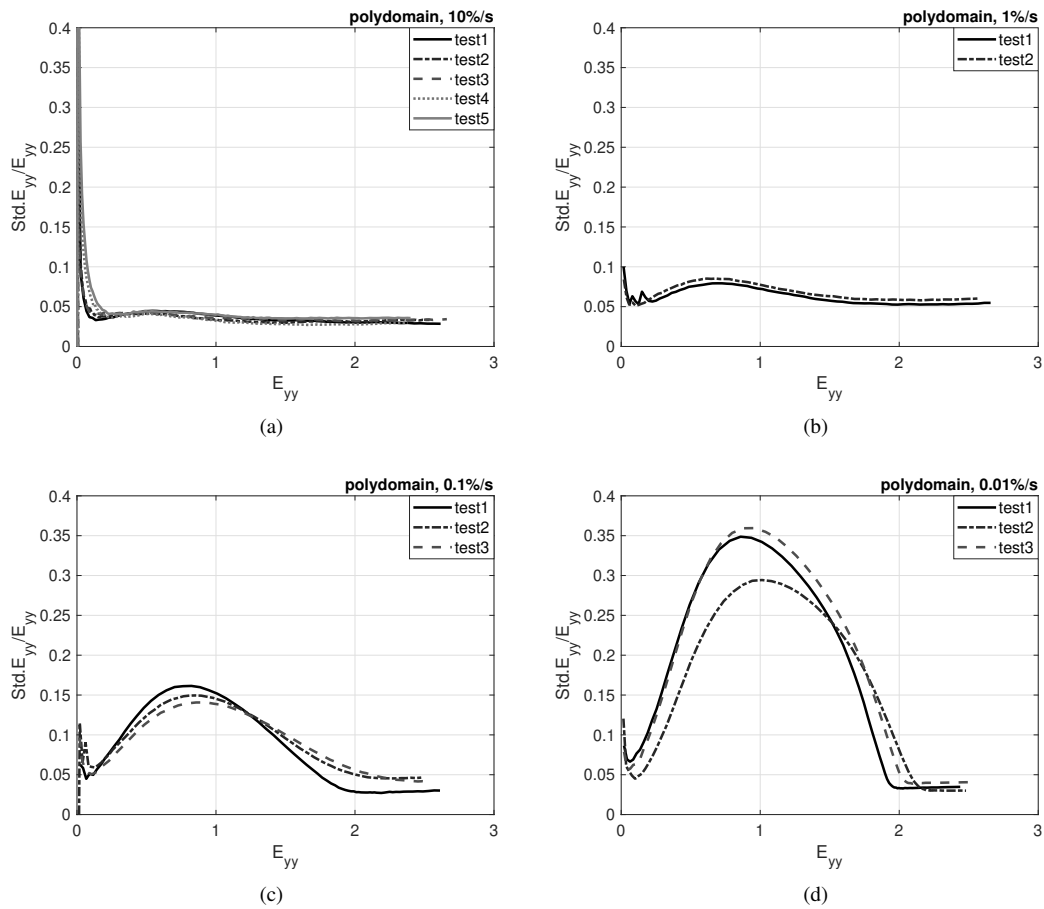
Figure S13: Standard deviation of the Green-Lagrange axial strain E_{yy} from 3D DIC normalized by the specimen-averaged E_{yy} for all the tests at different strain rates for polydomain. The normalized standard deviation is repeatable from test to test at each strain rate and variability between tests is smaller than the variability due to strain rate differences.
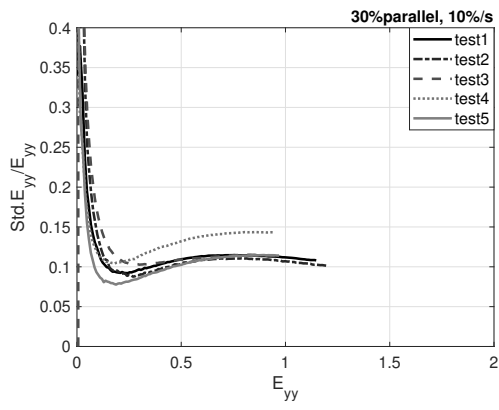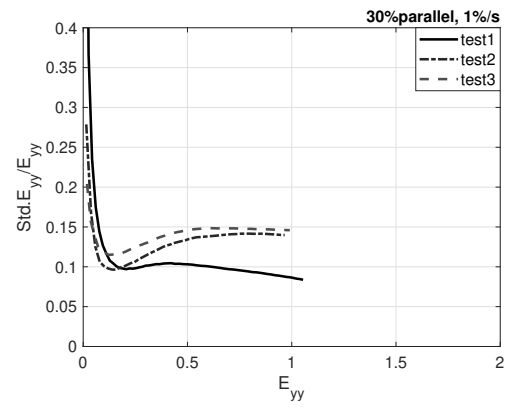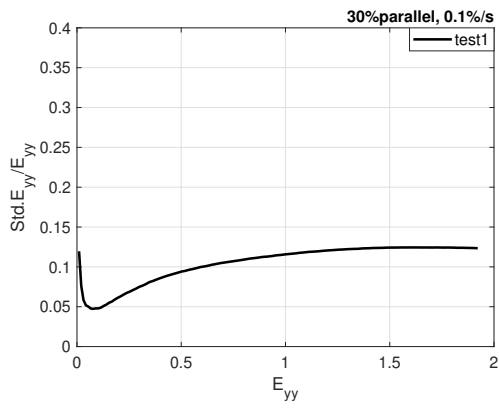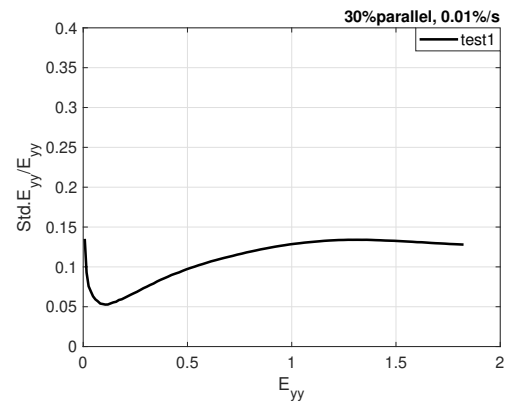
Figure S14: Standard deviation of the Green-Lagrange axial strain E_{yy} from 3D DIC normalized by the specimen-averaged E_{yy} for all the tests at different strain rates for 30% parallel. The normalized standard deviation is repeatable from test to test at each strain rate and variability between tests is smaller than the variability due to strain rate differences.
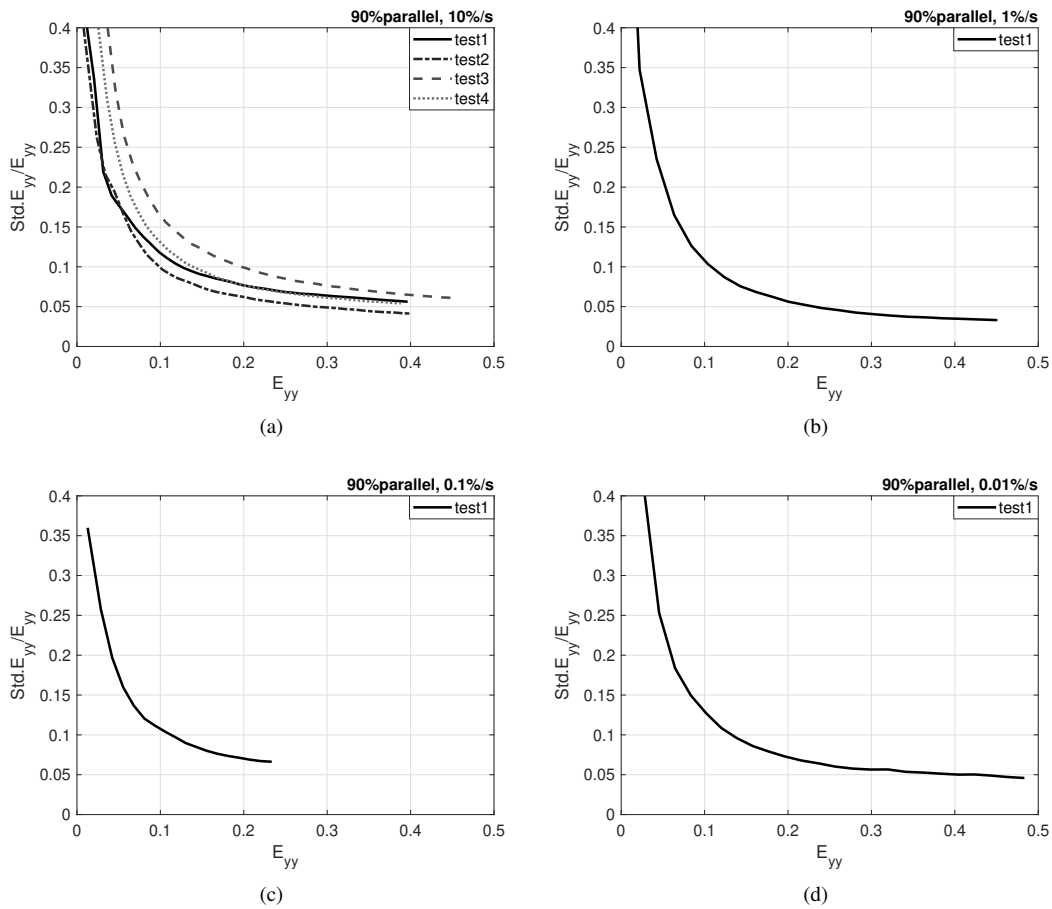
Figure S15: Standard deviation of the Green-Lagrange axial strain E_{yy} from 3D DIC normalized by the specimen-averaged E_{yy} for all the tests at different strain rates for 90% parallel. The normalized standard deviation is repeatable from test to test at each strain rate and variability between tests is smaller than the variability due to strain rate differences.
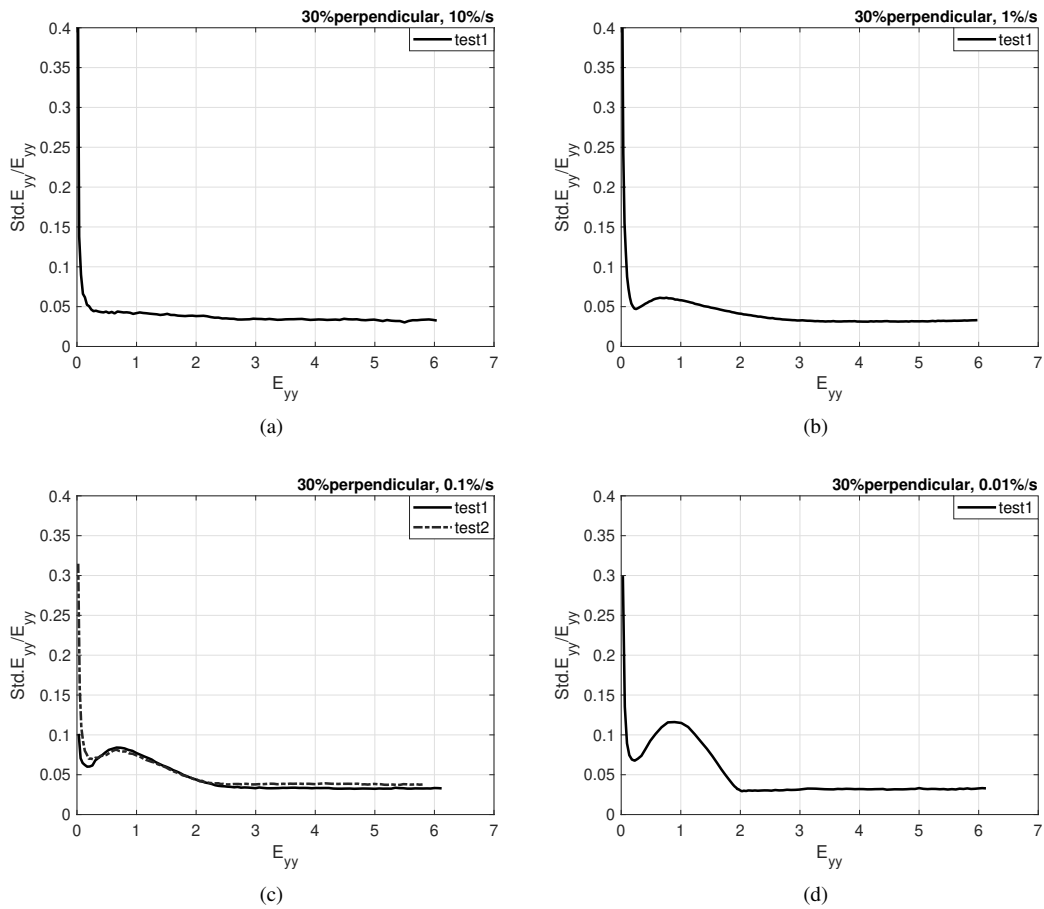
Figure S16: Standard deviation of the Green-Lagrange axial strain E_{yy} from 3D DIC normalized by the specimen-averaged E_{yy} for all the tests at different strain rates for 30% perpendicular. The normalized standard deviation is repeatable from test to test at each strain rate and variability between tests is smaller than the variability due to strain rate differences.
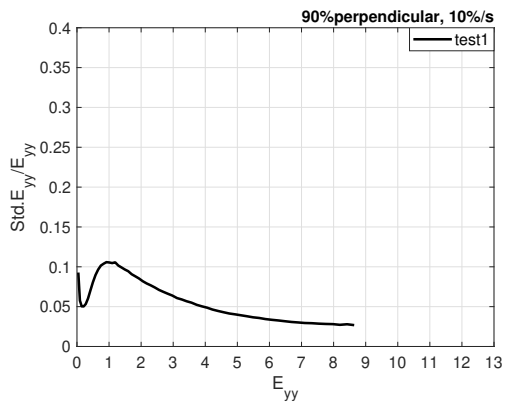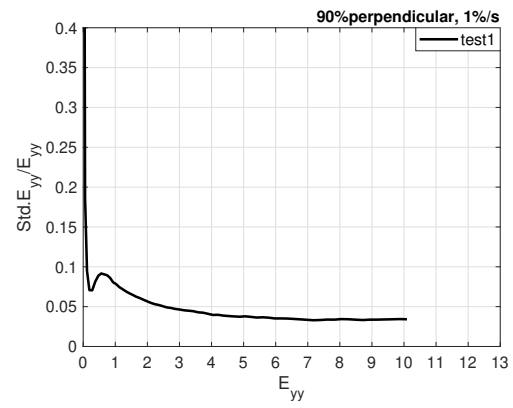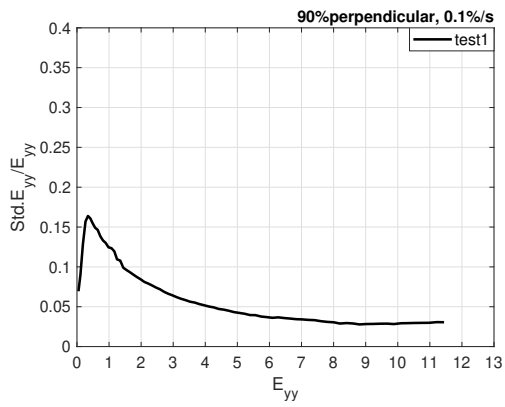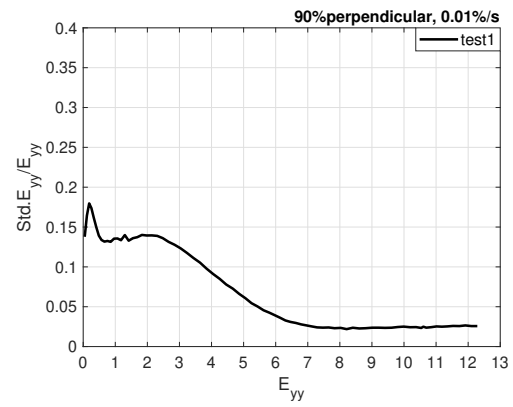
Figure S17: Standard deviation of the Green-Lagrange axial strain E_{yy} from 3D DIC normalized by the specimen-averaged E_{yy} for all the tests at different strain rates for 90% perpendicular. The normalized standard deviation is repeatable from test to test at each strain rate and variability between tests is smaller than the variability due to strain rate differences.

19